DOI: 10.1002/chem.200600402

Two Methods for the Determination of Enantiomeric Excess and Concentration of a Chiral Sample with a Single Spectroscopic Measurement

Lei Zhu, Shagufta H. Shabbir, and Eric V. Anslyn*[a]

Abstract: The previously established enantioselective indicator–displacement assays (eIDAs) for the determination of concentration and enantiomeric excess (*ee*) require two spectroscopic measurements for each chiral sample. To further simplify the operation of eIDAs, we now introduce two innovative analytical methods, both of which utilize a dual-chamber quartz cuvette, which reduces the number of spectroscopic measurements from two to one. An attractive feature of this cuvette is that the concentration- and *ee*-dependent absorption data can be collected at the isosbestic points or transparent regions of the spectra recorded in each individual chamber, thereby reflecting optical changes that occur in the other chamber. Therefore, two independent equations, which are needed to solve the values of the two independent variables—concentration and *ee*—can be established with only a single spectroscopic measurement. The first method takes advantage of this feature in conjunction with a judicious choice of indicator/host combinations to generate concentration- and *ee*-dependent calibration curves. Our second method removes the requirement to measure equilibrium constants and molar absorptivities altogether through the use of artificial neural networks (ANNs). The most frequently used three-layer feed-forward network is generated, which relates the absorption data to concentration and *ee* of the samples by training with a back propagation procedure. Here, the data collection is not limited to the isosbestic points or transparent regions. Both approaches enabled accurate and rapid determination of concentration and *ee* of chiral samples. The technology removes the relative difficulty, which is the need for two separate measurements for concentration and *ee* respectively, of analyzing chiral samples compared to achiral samples. When implemented in a high-throughput format, this technology should greatly facilitate the discovery of asymmetric catalysts in the same way as conventional high-throughput screening assays.

Keywords: analytical methods · artificial neural networks · chirality · host–guest systems · supramolecular chemistry

Introduction

Library screening approaches for the development of asymmetric catalysts are becoming standard protocols in both industry and academia[1,2] for rapid quantification of yield and enantiomeric excess (*ee*) of chiral products in a high-throughput fashion.[3,4] Currently, parallel chromatographic methods are mostly employed for that purpose.[5–9] The development of optical spectroscopic assays (e.g. absorption or fluorescence) should ease the instrumentation dependence and increase the speed of high-throughput assays.[1,10]

We introduced the use of enantioselective indicator-displacement assays (eIDAs) to determine both concentration and *ee* of chiral samples.[11–13] Few other methods have been shown to have this capacity.[14–17] In an eIDA, two spectroscopic measurements are taken. First, the concentration of a chiral sample ($[G]_t$) is determined with an indicator-displacement assay (IDA)[18] using an achiral host (H, Scheme 1). Second, an eIDA is carried out where a chiral host (H*) is used to generate a $[G]_t$- and *ee*-dependent optical signal (ΔAbs or F/F_I). Such a signal is related to $[G]_t$ and *ee* by way of a mathematical function of solution equilibrium constants and molar absorptivities ([Equation (2)], Scheme 1).[11] Because $[G]_t$ is known from the measurement using the achiral host H, the *ee* of the sample can be obtained by solving Equation (2). We have used an arylboronic acid based eIDA to quantitatively analyze chiral α-hydroxycarboxylates and diols.[11,12] The accuracies for both concentration and *ee* are well within the requirement for a typical asymmetric catalysis screening project.

[a] Dr. L. Zhu, S. H. Shabbir, Prof. Dr. E. V. Anslyn
Department of Chemistry and Biochemistry
The University of Texas at Austin, Austin, TX 78712 (USA)
Fax: (+1) 512-471-8696
E-mail: Anslyn@ccwf.cc.utexas.edu

IDA with an achiral receptor/host H

$$H{:}I + G \rightleftharpoons H{:}G + I \qquad K_{HI}/K_{HG}$$

$$\Delta Abs \text{ or } F/F_I = F_1([G]_t) \qquad (1)$$

IDA with a chiral receptor/host H*

$$H^*{:}I + G_R \rightleftharpoons H^*{:}G_R + I \qquad K_{H^*G_R}/K_{H^*I}$$

$$H^*{:}I + G_S \rightleftharpoons H^*{:}G_S + I \qquad K_{H^*G_S}/K_{H^*I}$$

$$\Delta Abs \text{ or } F/F_I = F_1([G]_t, ee) \qquad (2)$$

Scheme 1. Two-step enantioselective indicator-displacement assays (eIDAs). H: achiral host; H*: chiral host; I: indicator; G, G_R, G_S: guest; ΔAbs: absorbance change; F: fluorescence intensity; F_I: fluorescence intensity of an unbound indicator, a constant; $[G]_t$: guest concentration; *ee*: enantiomeric excess. K_{HI}, K_{HG}, K_{H^*I}, K_{H^*GR}, and K_{H^*GS} are affinity constants between host (H, H*) and substrates (I, G, G_R, G_S), respectively. Equation (1) is an empirical polynomial fit for an A versus $[G]_t$ displacement curve. Equation (2) is a theoretical function derived from solution multi-equilibria and Beer's Law analysis, shown here: $\{A-\varepsilon_I b[I]_t/b\text{-}(\varepsilon_{H^*I}-\varepsilon_I)\} + \{\varepsilon_I b[I]_t - A/K_{H^*I}(A-\varepsilon_{H^*I} b[I]_t)\} + \{K_{H^*GR}[G]_t(1+ee)\text{-}(\varepsilon_I b[I]_t - A)/2[A(K_{H^*I}-K_{H^*GR}) - b[I]_t(\varepsilon_{H^*I}K_{H^*I} - \varepsilon_I K_{H^*GR})]\} + \{K_{H^*GS}[G]_t\text{-}(1-ee)(\varepsilon_I b[I]_t - A)/2[A(K_{H^*I}-K_{H^*GS}) - b[I]_t(\varepsilon_{H^*I}K_{H^*I} - \varepsilon_I K_{H^*GS})]\} = [H]_t$.

The requirement for applying two spectroscopic measurements for analyzing one chiral sample prompted us to engineer the eIDA system further to eliminate the need for separate measurements for concentration and *ee*. We now report two critical improvements. The first is a reduction of the number of measurements from two to one by using a dual-chamber quartz cuvette (Figure 1 A).[19] A single absorption spectrum of the dual-chamber cuvette represents a combined optical response from each individual chamber caused by the addition of a chiral sample. The absorption data can be collected at the isosbestic points or alternate transparent region of the individual chambers, thus reflecting optical changes that take place in the other chamber. The consequence here is that two independent equations can be established by using data collected from a single spectroscopic measurement to determine the values of two independent variables (concentration and *ee*) in these two equations. In an extension of our mathematical procedure mentioned above, we describe a judicious choice of indicator/host combinations that takes advantage of this feature to generate both concentration- and *ee*-dependent calibration curves. Our second improvement uses the same dual-chamber cuvette to collect absorption data. However, we remove the requirement to measure equilibrium constants and molar absorptivities altogether by the use of an artificial neural network (ANN), for which the data collection is not limited to just isosbestic points and transparent regions. We demonstrate both approaches using the previously reported boronic acid receptors **1** and (*S,S*)-**2** (Figure 1).[11] The work reported here represents a significant advancement in the accuracy and more importantly, the speed of our eIDAs methodologies.

Results and Discussion

In the first approach, appropriate indicator/host combinations are added in respective chambers of the cuvette so

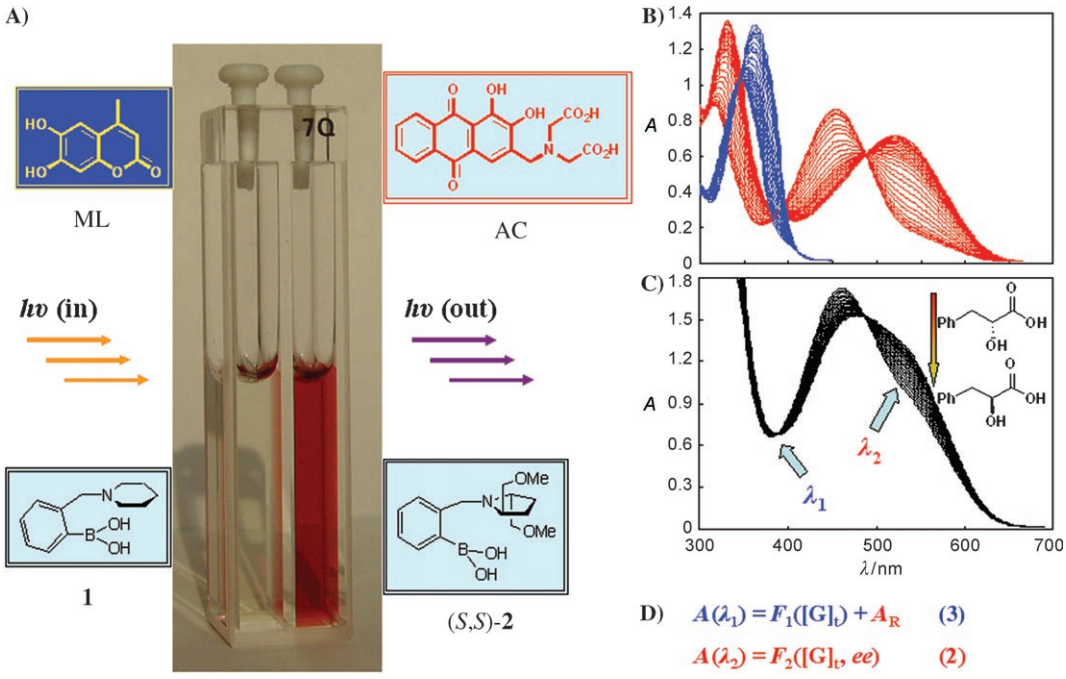

Figure 1. A) A dual-chamber quartz cuvette containing indicators ML (left) and AC (right). B) Overlay of two indicator–host isotherms. Blue: absorption spectra of ML (92.0 μM) in 75% methanolic aqueous solution buffered with 10 mM HEPES at pH 7.4 (default buffer) in the presence of (0–0.44 mM) of **1**; Red: absorption spectra of AC (115 μM) in the default buffer in the presence of (0–0.26 mM) of (*S,S*)-**2**. C) Absorption spectra of ML (198 μM), **1** (0.559 mM), AC (285 μM), and (*S,S*)-**2** (0.765 mM) in their designated chambers in the default buffer in the presence of PL (6.0 mM) with *ee* of D-PL varying from −1 to 1. D) Two independent equations that correlate the absorbance (A) to $[G]_t$ and *ee* at wavelengths λ_1 (387 nm) and λ_2 (536 nm).

that two independent equations regarding $[G]_t$ and *ee* can be established simultaneously with a single absorption measurement. The left chamber of the cuvette contained the achiral host **1** (H) and the colorless indicator 4-methylesculetin (ML); while the right chamber contained the chiral host (*S,S*)-**2** (H*) with the colorimetric indicator alizarin complexone (AC, Figure 1). Absorption modulations occur when the catechol-based ML and AC reversibly interact with boronic acid host **1** and (*S,S*)-**2**. The addition of the chiral α-hydroxycarboxylate phenyllactate (PL) enantioselectively alters the ratio of free and chiral host-bound indicators ([I] and [H*I]), hence also the absorbance.

A particularly attractive feature of this cuvette is that absorption data can be collected at the isosbestic points, or transparent regions, of the spectra recorded in each individual chamber, thereby only reflecting optical changes that occur in the other chamber. The absorption spectra of ML/**1** (blue) and AC/(*S,S*)-**2** (red) titration experiments are overlaid in Figure 1B. The isosbestic point of AC at 387 nm (λ_1) overlaps with a receptor-responsive region of ML that has a large dynamic range. At 387 nm, the absorbance from the right chamber (A_R) is independent of both host ([H*]) and guest ($[G]_t$) concentrations, whereas the absorbance from the left chamber is only dependent on the guest concentration ($[G]_t$) because the residing host in the left chamber (**1**) is achiral. By combining the absorbance from both chambers at this wavelength, Equation (3) is established (Figure 1D). In contrast, at 536 nm (λ_2) where the indicator ML is transparent, the absorbance change is solely due to the chemical events taking place in the right chamber. The absorbance is dependent on both $[G]_t$ and *ee* because the right chamber is occupied by the chiral host (*S,S*)-**2** [Eq. (2)]. Putting these two equations together, the values of $[G]_t$ and *ee* can be solved. The overall spectroscopic modulation with the *ee* of PL ranging from −1 to 1, where the concentration of PL is fixed at 6.0 mM, is plotted in Figure 1C.

The parameters required for Equations (2) and (3) (A_R, K_{H*I}, ε_I, ε_{H*I}, K_{H*GR}, K_{H*GS}, $[I]_t$, $[H^*]_t$, I = AC) are determined independently prior to the actual analysis. In short, the equilibrium constants and molar absorptivities (K_{H*I}, ε_I, ε_{H*I}, K_{H*GR}, K_{H*GS}) were determined by UV/Vis titrations in the dual-chamber cuvette (b = 0.5 cm, while the other chamber was filled with buffer blank in these parameter-determination experiments) using entiomerically pure PL samples (for experimental procedures see reference [11]). A_R was also determined from the above-mentioned titrations by averaging the absorption values at 387 nm when AC was used as the indicator at (284.5 μM). The total concentration values ($[I]_t$, $[H^*]_t$) were determined gravimetrically.

A calibration curve for $[G]_t$ determination was generated as the following: A displacement isotherm at 387 nm was afforded by titrating PL (either enantiomer, 0–6.55 mM) into a solution of the achiral host **1** (0.307 mM) and indicator ML (202 μM) in the left chamber of the cuvette (the right chamber was filled with buffer). The isotherm was raised by adding A_R [Eq. (3)]. As described before, A_R is the absorbance at the isosbestic point (387 nm) of AC at the concentration of AC used in the right chamber (284.5 μM), which was determined to be 0.31. The empirical polynomial curve fitting afforded the A_{387} versus $[G]_t$ relationship Equation (3) as $y = 8\times10^{-6}x^6 - 0.0002x^5 + 0.0028x^4 - 0.0181x^3 + 0.0727x^2 - 0.2043x + 1.0318$ (y = A, $x = [G]_t$). The high-order (6th) of the polynomial curve fitting allowed us to gain the maximum regression coefficient ($R^2 = 1$). This equation was subsequently used as a calibration equation for the accurate determination of $[G]_t$ (Figure 2B).

Three *ee* titration experiments were performed in the dual-chamber cuvette by using the 2-indicator-2-host system.[19] For each set of data, the concentration of PL ($[G]_t$) was fixed and the *ee* of D-PL was varied from −1 to 1. The actual titration spectra are similar to the ones shown in Figure 1C. The absorbance at 387 nm versus *ee* values for all three sets of spectra is shown in Figure 2A. As expected, the absorbance at 387 nm is independent of *ee* values. However, it differs with respect to total concentration $[G]_t$ (Figure 2A). The average absorbance values for each $[G]_t$ value are overlaid with the calibration curve at 387 nm (Figure 2B). The predictive power of the calibration curves is evident. The concentrations $[G]_t$ of 11 designated unknown PL samples (the "unknown" samples were randomly chosen from the three titration experiments). These 11 data points were not included in the three calibration curves in Figure 3, but instead were determined by solving Equation (3) using

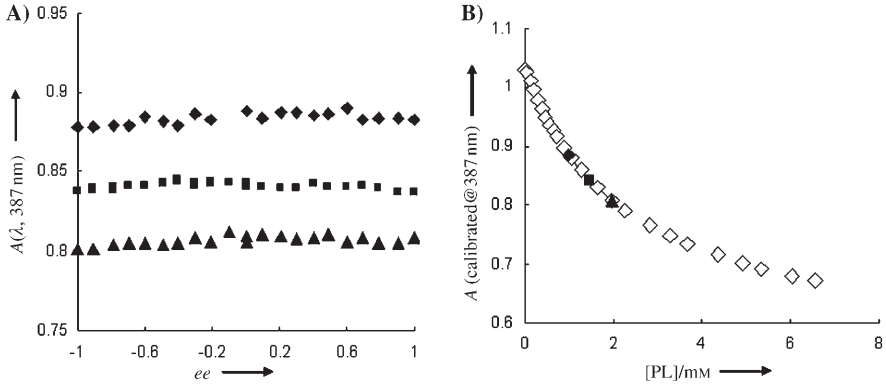

Figure 2. A) Absorbance change at 387 nm of ML (202 μM), **1** (307 μM), AC (284.5 μM), and (*S,S*)-**2** (400 μM), in their designated chambers in the default buffer, upon increasing *ee* of D-PL. ◆: $[G]_t$ = 0.98 mM. ■: $[G]_t$ = 1.47 mM. ▲: $[G]_t$ = 1.96 mM. B) ◇: the absorbance change at 387 nm of the dual-chamber ensemble in Figure 2A upon increasing concentration of L-PL (D-PL produced an identical curve, not shown). The average absorbance from the *ee* titrations (coding scheme as in Figure 2A) at three different $[G]_t$ values are overlaid on the calibration curve.

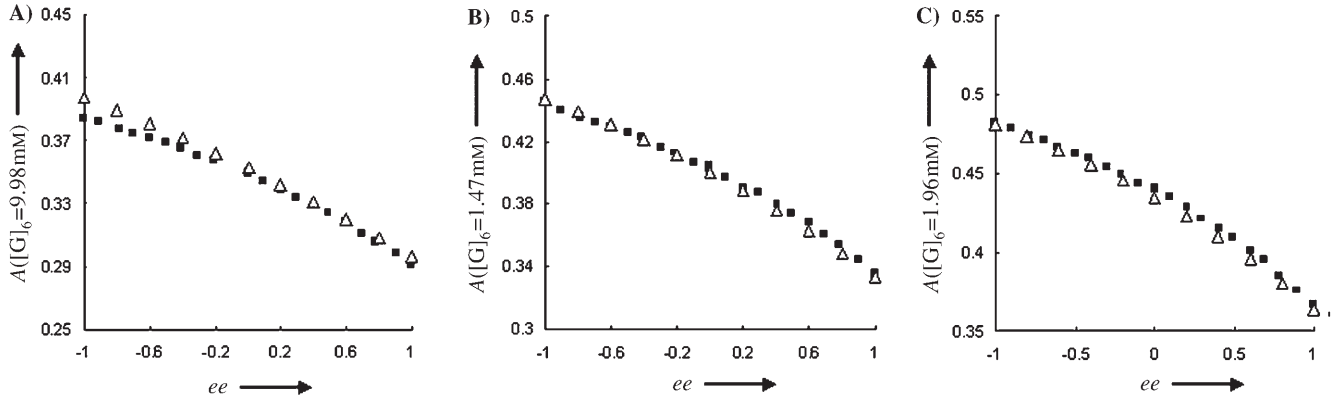

Figure 3. ■: absorbance changes at 536 nm of the dual-chamber ensemble upon increasing *ee* of D-PL. A) $[G]_t = 0.98$ mM; B) $[G]_t = 1.47$ mM; C) $[G]_t = 1.96$ mM. △: data calculated from Equation (2) by the computer program Mathematica 5.1.[21]

the software Mathematica 5.1.[20] The average absolute errors were limited to an average of ±3.3% (Table 1).

Table 1. Determination of concentration and *ee* of PL samples. IA: determined by isosbestic point analysis; ANN: determined by artificial neural network. % *R*: the percentage of *R* (D-PL) in the samples.

No.	$[G]_t$ [mM] (actual)	$[G]_t$ [mM] (IA)	$[G]_t$ [mM] (ANN)	*ee*/% *R* (actual)	*ee* (IA)	% *R* (ANN)
1	0.98	1.06	0.98	−0.90/5	−0.42	4
2	0.98	1.03	0.98	−0.49/25	−0.22	24
3	0.98	0.97	0.99	0.00/50	0.03	48
4	0.98	1.00	0.98	0.90/95	1.00	94
5	1.47	1.54	1.47	−1.00/0.00	−0.82	−2
6	1.47	1.46	1.47	−0.30/35	−0.31	35
7	1.47	1.50	1.47	0.49/75	0.46	75
8	1.96	2.06	1.96	−0.69/15	−0.61	14
9	1.96	1.92	1.93	−0.10/45	−0.21	43
10	1.96	1.98	1.96	0.69/85	0.62	84
11	1.96	1.96	1.95	0.10/55	0.00	54

The absorbance at 536 nm, where the bound indicator (H*I) absorbs, with regard to *ee* values at three different $[G]_t$ values are plotted in Figure 3. At a fixed $[G]_t$ value, the absorbance decreases (which indicates that the amount of free indicator AC is reduced) with increasing *ee* of D-PL, the enantiomer with lesser affinity. When the $[G]_t$ found from the measurement in the first chamber is used in Equation (2), only a function of *ee* is obtained. Calculated *A* versus *ee* curves were generated for the three $[G]_t$ values as shown in Figure 2. The overlay of the theoretical predictions with the experimental *ee* data for all three $[G]_t$ cases is shown in Figure 3.[21] Equation (2) was then used to determine the *ee* of the 11 unknown PL samples, where their concentrations ($[G]_t$) were determined by Equation (3). The average absolute error of the *ee* determination was ±7.9% (Table 1).[22] Hence, the determination of both $[G]_t$ and *ee* of chiral samples using single spectroscopic measurements is possible using a dual-chamber cuvette.

The second approach relies on an analysis using artificial neural networks (ANNs). An ANN is an information processing paradigm that simulates the way biological nervous systems, in particular the brain, process information. The computer programs that implement the ANN paradigm are able to solve problems by learning from analogous existing examples. The theoretical foundation and the applications of ANNs in chemistry, mainly in the pattern recognition area, have been extensively reviewed.[23,24]

The chiral analysis problem in this study can be solved with an ANN program. The general procedure included three steps. First, the absorbance data obtained with known $[G]_t$ and *ee* values are fed into the program. A network is subsequently generated that accurately models the unknown underlying function that relates the input variables to the output variables. Second, a successful training session establishes a hidden function in the form of $\{[G]_t, ee\} = F(A_{\lambda 1}, A_{\lambda 2}, A_{\lambda 3}$, etc.) within the network. Third, absorbance data from test samples are input into the network. After the new data are processed by the hidden function, the network will generate outputs, which in this case are the values of $[G]_t$ and *ee*.

As a simple demonstration, the absorbance at 387 nm and 536 nm (A_{387}, A_{536}) from the three *ee* titrations and corresponding $[G]_t$ and %*R* (the percentage of *R*(D)-PL in the sample)[25] values, excluding the 11 data points in Table 1, were used as training sets. A_{387} and A_{536} were considered as inputs, and $[G]_t$ and %*R* were outputs. Thus, a total of 65 cases were imported into the Statistica Neural Networks 4.0 program,[26] 10 of these cases were randomly selected by the program for the cross-verification of the networks that are generated. In principle, a large number of networks are tested and the one with the best cross-verification error is selected. The Statistica Neural Networks program has an embedded intelligent problem solver (IPS) function, which is used to automatically create a network set that contains neural networks suitable for the designated problem. From the network set, a multilayer perceptron (MLP) with two inputs was selected based upon both its performance rating and our experience with the MLP type of neural networks (Figure 4 A).[27,28] The selected MLP was subsequently trained with the back-propagation algorithm. Thereafter, the

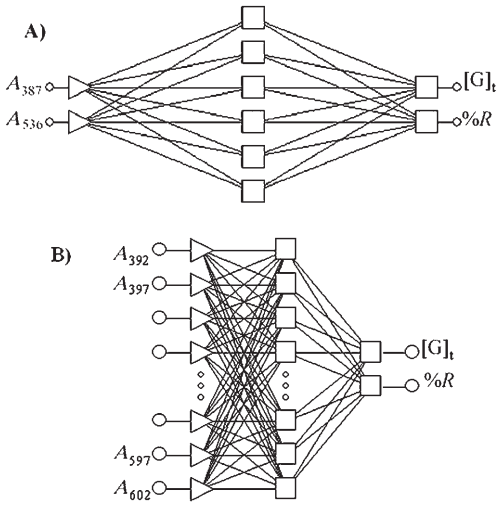

Figure 4. Structures of two MLP networks in this study. Both have three layers: A) the input layer on the left has two variables—A_{387} and A_{536}. The input layer is connected to, and processed by a hidden layer in the middle with six nodes. Two variables, $[G]_t$ and $\%R$, are generated to the output layer on the right; B) the input layer has 43 variables from A_{392} to A_{602} at 5-nm intervals. The hidden layer has 11 nodes.

learning process of the MLP network was completed and a hidden function with predictive power specifically tailored for our problem was established.

For unknown sample analysis, the trained network was switched to run "one-off" cases. The "one-off" case is a function of the ANN program that takes a new input to generate an output by the trained network. Two absorbance values, A_{387} and A_{536}, of the designated 11 unknown data were fed to the network to generate the output $[G]_t$ and $\%R$. The predicted $[G]_t$ and $\%R$ values for the 11 unknown samples are shown in Table 1 with average absolute errors of $\pm 0.45\%$ and $\pm 1.1\%$, respectively. However, strictly speaking, these unknown values are not technically unknown because they were obtained in the same set of titration experiments from which the training sets of data were generated. The trained MLP network should be able to predict $[G]_t$ and *ee* from independently prepared and measured samples, which would be true unknowns.

Thus, to test the capability of the ANN-based model to respond to true unknown samples, we examined samples never used in network development. A new MLP network was generated with only two *ee* training sets at two different $[G]_t$ values (0.98 mM and 1.96 mM). In this analysis, one independently determined *ee* data set with $[G]_t$ at 1.47 mM was used to represent unknown samples. The new network was constructed with absorbance values at 43 wavelengths, instead of two, as inputs in order to enhance the quality of the trained network. Again, a network set was successfully generated by IPS, consisting of 34 training sets and seven validation sets. The network with the best performance (structure in Figure 4B) was trained with a back-propagation algorithm. The $[G]_t$ and $\%R$ of five samples from the data set with actual $[G]_t$ at 1.47 mM were predicted by the trained network within 11.4% and 4.2% average absolute errors, respectively, of the actual values (Table 2). Considering that the testing samples were prepared and data were collected

Table 2. Determination of concentration and $\%R$ of PL samples with a trained MLP network (Figure 4B). $[G]_t$ (actual) = 1.47 mM.

$\%R$ (actual)	20	45	75	50	100
$\%R$ (determined)	27	50	79	52	103
$[G]_t$ [mM] (determined)	1.62	1.58	1.58	1.57	1.57

under entirely independent conditions from those of the training set data, it is amazing that the ANN gained such predicting ability through learning. The relatively low accuracy in $[G]_t$ determination (determined average at 1.58 mM versus the actual value of 1.47 mM) should be attributed to the lack of $[G]_t$ variations in the training set data. The accuracy will certainly increase should a larger body of training set data be used. Admittedly, the ANN study reported herein is a proof-of-principle demonstration of the promise as well as the limitation of analytical protocols based on ANNs. In a practical implementation, more data than used in this study would be needed to train the networks.

The advantages of ANNs over the traditional spectroscopic approach based upon the analysis of solution thermodynamics and Beer's Law in determining concentration and $\%R$ (or *ee*) of a chiral sample are obvious. What is required for implementing an ANN analysis is simply a large body of existing data (training sets) that represent the behavior of the system of interest (the spectroscopic modulation with regard to $[G]_t$ and $\%R$), and a computer program (Statistica Neural Networks) that can model and predict behavior of the system that is not included in the existing data. Thus, the laborious determination of thermodynamic and optical parameters is not needed, and the indicator choice and wavelengths for analysis are not as restricted as in the isosbestic analysis. Furthermore, the ANN approach described in this study can be extended to other mixture analysis amenable to indicator-displacement assays. However, one drawback of ANN analysis is that a large body of existing data has to be available. ANNs are at their best when they are trained with rich information for the system under study.

Conclusion

In summary, we have developed two different approaches for the determination of concentration $[G]_t$ and *ee* of a chiral sample with a single spectroscopic measurement. The analysis of PL samples by eIDAs based on a chiral boronic acid host was used to demonstrate the described methods. The experimental setup for both methods relies on a cuvette with two separate chambers. In practice, two independent IDAs, one of which used a chiral host, were carried out simultaneously with the addition of identical guest samples in both chambers. In the first approach, an isosbestic analysis

led to the establishment of two independent equations for solving two desired variables $[G]_t$ and *ee*. In the second approach, an artificial neural network (ANN) analysis was used for determining $[G]_t$ and $\%R$. Both approaches achieved satisfactory accuracy. The implementation of either approach will be determined by particular applications and/or practitioner's preferences. Both approaches are naturally extendable to high-throughput formats, potentially by using designer multi-well absorbance plate readers that simulate double-chamber cuvettes.

Experimental Section

Typical procedure for double-chamber cuvette *ee* titration: Four ensemble solutions (A–D) were prepared. Their respective compositions are: solution A: ML (202 μM), **1** (307 μM), D-PL (0.982 mM); solution B: ML (202 μM), **1** (307 μM), L-PL (0.982 mM); solution C: AC (284 μM), (*S,S*)-**2** (400 μM), D-PL (0.982 mM); solution D: AC (284 μM), (*S,S*)-**2** (400 μM), L-PL (0.982 mM). Solutions B and D (500 μL each) were added into the left and right chambers of the cuvette, respectively. Solutions A and C were incrementally titrated into the left and right chambers, respectively, until 500 μL each of A and C were added, where the *ee* of PL reached 0 in both chambers. The absorption spectrum was recorded three minutes after each addition to allow the system to reach equilibrium. The titration was repeated with solutions B and D adding into solutions A and C in their respective chambers to complete the *ee* range from −1 to 1.

ANN training procedure: Among 65 data in the training set, 55 were designated as training data by the Statistica program, the remaining 10 data were designated as verification data. The IPS was requested to search for MLP networks with three layers, input, hidden, and output, respectively. One search sequence was designed to last for two minutes, during which the number of units in the hidden layer was varied until the best network was found. The found network, which has six hidden layer units, was trained with a back-propagation algorithm until the errors of training and verification data converged at ~1%.

Acknowledgements

We thank Dr. Pierre N. Floriano for helpful discussions. This work was supported by NIH (1 R01 GM077437) and the Welch Foundation (F-1151).

[1] M. T. Reetz, *Angew. Chem.* **2001**, *113*, 3701–3703; *Angew. Chem. Int. Ed.* **2001**, *40*, 284–310.
[2] D. Wahler, J.-L. Reymond, *Curr. Opin. Chem. Biol.* **2001**, *5*, 152–158.
[3] M. Tsukamoto, H. B. Kagan, *Adv. Synth. Catal.* **2002**, *344*, 453–463.
[4] M. G. Finn, *Chirality* **2002**, *14*, 534–540.
[5] C. J. Welch, T. Szczerba, S. R. Perrin, *J. Chromatogr. A* **1997**, *758*, 93–98.
[6] C. J. Welch, B. Grau, J. Moore, D. J. Mathre, *J. Org. Chem.* **2001**, *66*, 6836–6837.
[7] C. J. Welch, F. Fleitz, F. Antia, P. Yehl, R. Waters, N. Ikemoto, I. J. D. Amstrong, D. J. Mathre, *Org. Process Res. Dev.* **2004**, *8*, 186–191.
[8] M. S. Sigman, E. N. Jacobsen, *J. Am. Chem. Soc.* **1998**, *120*, 4901–4902.
[9] C. Wolf, P. A. Hawes, *J. Org. Chem.* **2002**, *67*, 2727–2729.
[10] M. T. Reetz, *Angew. Chem.* **2002**, *114*, 1391–1394; *Angew. Chem. Int. Ed.* **2002**, *41*, 1335–1338.
[11] L. Zhu, E. V. Anslyn, *J. Am. Chem. Soc.* **2004**, *126*, 3676–3677.
[12] L. Zhu, Z. Zhong, E. V. Anslyn, *J. Am. Chem. Soc.* **2005**, *127*, 4260–4269.
[13] J. F. Folmer-Andersen, V. M. Lynch, E. V. Anslyn, *J. Am. Chem. Soc.* **2005**, *127*, 7986–7987.
[14] F. Taran, C. Gauchet, B. Mohar, S. Meunier, A. Valleix, P. Y. Renard, C. Crèminon, J. Grassi, A. Wagner, C. Mioskowski, *Angew. Chem.* **2002**, *114*, 132–135; *Angew. Chem. Int. Ed.* **2002**, *41*, 124–127.
[15] Y. Chen, K. D. Shimizu, *Org. Lett.* **2002**, *4*, 2937–2940.
[16] Z. Li, L. Bütikofer, B. Witholt, *Angew. Chem.* **2004**, *116*, 1730–1734; *Angew. Chem. Int. Ed.* **2004**, *43*, 1698–1702.
[17] S. Dey, K. R. Karukurichi, W. Shen, D. B. Berkowitz, *J. Am. Chem. Soc.* **2005**, *127*, 8610–8611.
[18] S. L. Wiskur, H. Aït-Haddou, J. J. Lavigne, E. V. Anslyn, *Acc. Chem. Res.* **2001**, *34*, 963–972.
[19] Starna Cells, Inc.
[20] http://www.wolfram.com.
[21] Parameters used for solving Equation (2): $b = 0.5$ cm, $\varepsilon_I = 4600\,M^{-1}cm^{-1}$, $\varepsilon_{H*I} = 128\,M^{-1}cm^{-1}$, $K_{H*I} = 15000\,M^{-1}$, $K_{H*GR} = 2174\,M^{-1}$, $K_{H*GS} = 7142\,M^{-1}$, $[H^*]_t = 0.40 \times 10^{-3}\,M^{-1}$, $[I]_t = 284.5 \times 10^{-6}\,M^{-1}$. ε_I and ε_{H*I} values were slightly adjusted from values determined by AC and (*S,S*)-**2** 1:1 association titration experiment to gain satisfying curve fittings in Figure 3.
[22] The first two outliers, which lay on the least sensitive region of the *A* versus *ee* calibration curve, were excluded in the error determination.
[23] D. A. Cirovic, *TrAC Trends Anal. Chem.* **1997**, *17*, 148–155.
[24] J. A. Burns, G. M. Whitesides, *Chem. Rev.* **1993**, *93*, 2583–2601.
[25] "$\%R$" was used in ANN analyses instead of *ee* to avoid complications raised by minus numbers in statistical computations.
[26] StatSoft, Inc.
[27] S. L. Wiskur, P. N. Floriano, E. V. Anslyn, J. T. McDevitt, *Angew. Chem.* **2003**, *115*, 2116–2118; *Angew. Chem. Int. Ed.* **2003**, *42*, 2070–2072.
[28] S. C. McCleskey, P. N. Floriano, S. L. Wiskur, E. V. Anslyn, J. T. McDevitt, *Tetrahedron* **2003**, *59*, 10089–10092.

Received: March 21, 2006
Published online: October 26, 2006

